Materials Physics and Mechanics 16 (2013) 55-65 Received: December 9, 2012

HYBRID ENERGY HARVESTING FROM VIBRATION AND TEMPERATURE GRADIENT BY PZT AND PMN-0.25PT CERAMICS

Masoud Goudarzi[1*], Kamran Niazi[2], Mohammad Kazem Besharati[3]**

[1]Department of Mechanical Engineering, Razi University of Kermanshah, Iran

[2]Department of Mechanical Engineering, Science and Research branch, Islamic Azad University, Kermanshah, Iran

[3]Department of Mechanical Engineering, University of Tehran, Tehran, Iran

*e-mail: masoud.goudarzi@gmail.com

**e-mail: niazi8910@gmail.com

Abstract. Energy harvesting is the act of scavenging small amounts of power from the ambient energy resources. Such ambient energy can come from various green energy sources such as solar, thermal, wind, and kinetic energy. These amounts of energy can power up sensor nodes and therefore reduce the wiring complications or eliminate the need of changing batteries frequently. Two of the most popular methods for harvesting energy consisted of the application of piezoelectric and pyroelectric materials in scavenging energy from vibration and thermal gradients, respectively. This paper presents a hybrid harvesting technique by piezoelectric and pyroelectric effect, simultaneously. The concept of method and theoretical analysis is presented in details for parallel and series SSHI (synchronize switch harvesting on inductor). Numerical results are examined and show better performance compare with piezogenerators for PZT and PMN-0.25PT elements. In this paper it has been proven that hybrid energy harvesting energy by pyroelectric and piezoelectric effect, simultaneously, increases almost 38 % and 53 % more power as it does harvest by just piezoelectric effect. Followed by mentioned analyses the effect of three important parameters - temperature amplitude, vibration amplitude, and frequency- are examined. The more effective harvesting method and material is proposed in the final part of the paper.

1. Introduction

In line with the development of micro electro-mechanical systems (MEMS), providing energy in micro scale to feed these systems has gained much attention among researchers. Two conventional methods of energy supplying are (a) direct supply with wires or batteries and (b) converting ambient energy to electrical energy directly [1, 2]. In the past years, the use of separate energy sources connected wires had great popularity. This method was not desirable due to corrosion problems as well as maintenance issues. On the other hand, in the case of system complexity, not only the system size would become large due to using numerous wires, but basically, it would not be possible with these wireless systems [3, 4]. The implementation of batteries would be considered a superior way as the system size would be decreased and the production of wireless and mobile systems would easily be feasible. The main drawback of the method was the short life time of batteries that force regular replacement and maintenance costs [5, 6]. On the other hand, batteries usually die without prior alarm that is not desirable in security and safety monitoring applications, while

environmental pollutions resulting from disposal of batteries cannot be neglected [5-7]. Given the above difficulties, the best method for powering MEMS is the direct converting of ambient energy to electrical [8-10]. There are unlimited resources around us that could be converted directly into electrical energy, which could lead to a portable system and resolve existing problems of the mentioned methods. Some of the ambient energy resources, for instance, are light energy, electromagnetic energy, mechanical vibration and temperature gradients [11-14]. This study is focused on temperature gradients and mechanical vibration resources. Pyroelectric and piezoelectric are materials that generate an electrical voltage in response to thermal and vibration fluctuations respectively [15-18]. Two circuits that have been widely used during recent years are series and parallel SSHI circuits (synchronized switch harvesting on inductor). Their high efficiency compared with previous methods has been proven in the literature. The energy generated by these circuits is in micro-Watt scale when they are equipped with pyroelectric materials and in milliwatt scale when using piezoelectric substances [19-23]. The remainder of the paper is structured as follows: first these two circuits is introduced in hybrid form based on piezoelectricity and pyroelectricity effect. Furthermore, the efficiency of the hybrid method compared to the circuit implementing only piezoelectricity effect, has been discussed. Effective parameters in the energy harvesting circuits, namely, temperature amplitude, mechanical displacement, frequency and electrical quality factor are studied in the last section of the paper.

2. Energy harvesting device

The aim of this section is explaining the general principles of two energy harvesting processes from the piezoelectric and pyroelectric effect. These two harvesting circuits are parallel and series SSHI (synchronize switch harvesting on inductor). In each harvesting methods average harvested power is expressed as a function of frequency, electrical load and other parameters of the model.

2.1. Parallel SSHI. The method used throughout this paper called synchronized switch harvesting on the inductor (SSHI) has been extracted from the synchronized switch damping on the inductor (SSDI) which is a nonlinear method of vibration control. This Parallel-SSHI interface is comprised of a non-linear circuit connected in parallel with the smart element electrodes and the input of the rectifier bridge [4, 17], as shown in Fig. 1.

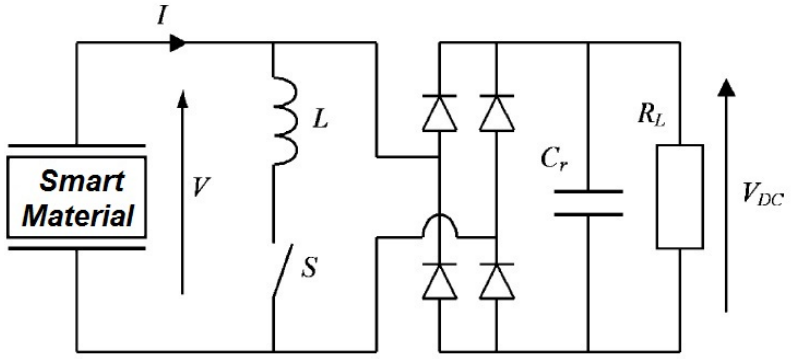

Fig. 1. Parallel-SSHI interface circuit.

This circuit is composed of an inductor L and an electronic switch S. The electronic switch is shortly turned on, at mechanical displacement's extremum. During these times, an oscillating electrical circuit L–C0 is launched. The period electrical oscillation is selected much smaller than the period of mechanical vibration T. After a half electrical period the switch is turned off, and it causes to voltage inversion. The theoretical temperature, displacement and voltage waveforms are presented in Fig. 2.

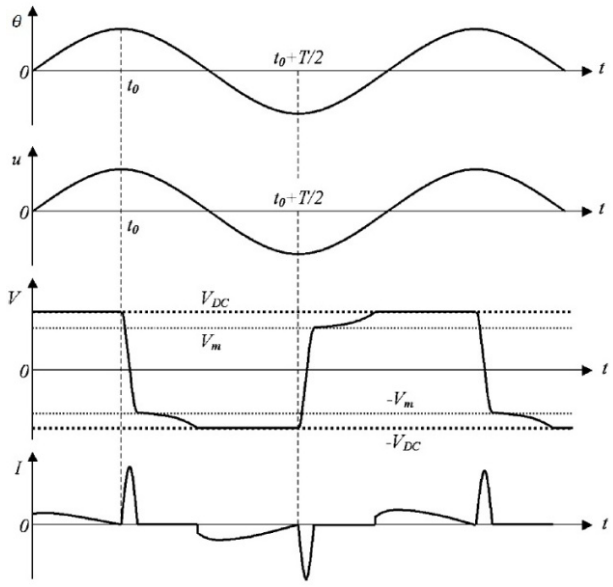

Fig. 2. Parallel-SSHI interface: displacement and voltage waveforms [4, 17].

The inversion of voltage is not perfect, meaning that always there are small energy losses in non-linear process. Most of the voltage inversion losses are due to the inductor and switch elements. These losses are modeled by the electrical quality factor Q_i of the circuit oscillator. The relation between Q_i and the voltages before (V_{DC})and after (V_m) is given in Eq. (1):

$$V_m = -V_{DC} e^{\frac{-\pi}{2Q_i}}. \tag{1}$$

Equation (2) shows the electric charges which terminal load equivalent resistor R_L Received during a half of mechanical periods. Where the second integral of that represents the sum of charge stored on the capacitor C_0 before and after the voltage inversion, which is given by Eq. (3). Also regarding to constitutive Equations of smart materials [5, 17] relation between mechanical and electrical variables is presented in Eq. (4).

$$\int_{t_0}^{t_0+\frac{T}{2}} I dt + \int_{t_0}^{t_0+\frac{T}{2}} I_s dt = \frac{V_{DC}}{R_L}\frac{T}{2}, \tag{2}$$

$$\int_{t_0}^{t_0+\frac{T}{2}} I_s dt = C_0 V_{DC}\left(1+e^{\frac{-\pi}{2Q_i}}\right), \tag{3}$$

$$I = \alpha_2 u'_m + \alpha_1 \theta'_m - c_0 V'_{DC}\ , \tag{4}$$

where α_1 and α_2 are dependent pyroelectric and piezoelectric properties:

$$\alpha_1 = \mathrm{PA}, \tag{5}$$

$$\alpha_2 = \frac{\mathrm{e}_{33}\mathrm{A}}{\mathrm{L}} \tag{6}$$

In these equations the parameters P, A, L, and e_{33} are, respectively, pyroelectric coefficient, the section and the thickness of the smart element, and piezoelectric coefficient. Integrating and combining Eqs. (2), (3) and (4) lead to the expression of the load voltage V_{DC} as a function of the displacement amplitude u_m and temperature amplitude θ_m which is shown in Eq. (7):

$$V_{DC} = \frac{2R_L\omega}{R_L C_0 (1+e^{\frac{-\pi}{2Q_i}})\omega + \pi}(\alpha_2 u_m + \alpha_1 \theta_m). \tag{7}$$

The average harvested power P is expressed in Eq. (8). This average harvested power P reaches a maximum value P_{max} by considering an optimal equivalent load resistance R_{opt}. Deriving of Eq. (8) results to maximum power and optimal equivalent resistance equations which are presented in Eqs. (8) and (9). These relations show that the harvested power, influenced by the voltage inversion efficiency, modeled by the electrical quality factor Q_i. This factor is practically restricted by the inductor's losses (Joule and ferromagnetic losses). In experimental set ups, the reported quality factor, is variable between Q_i = 0 and 13. To access this value more than 20 inductor losses must reach a very low amount. It causes to device bulkier, heavier and with expensive components

$$P = \frac{V_{DC}^2}{R_L} = \frac{4R_L\omega^2}{\left(R_L C_0 \omega (1-e^{\frac{-\pi}{2Q_i}}) + \pi\right)^2}(\alpha_2 u_m + \alpha_1 \theta_m)^2, \tag{8}$$

$$R_{opt} = \frac{\pi}{C_0 \omega (1-e^{\frac{-\pi}{2Q_i}})}, \tag{9}$$

$$P_{\max} = \frac{\omega}{\pi C_0 (1-e^{\frac{-\pi}{2Q_i}})}(\alpha_2 u_m + \alpha_1 \theta_m)^2. \tag{10}$$

2.2. Series SSHI. The circuit of Series-SSHI is similar to the Parallel- SSHI circuit, but place of connecting the {switch + inductor} in parallel with the smart element, is connected in series, as shown in Fig. 3.

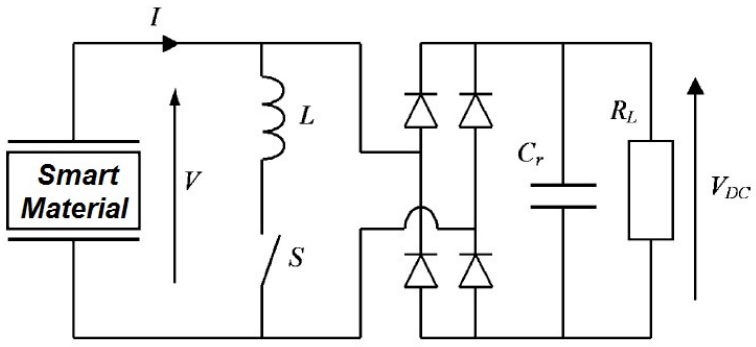

Fig. 3. Series-SSHI interface circuit.

The control of switching is the same as the Parallel-SSHI circuit. Most of the time, the switch is open except in proximity of mechanical displacement extremums. The inversion of voltage occurs in those moments. The temperature, voltages and displacement waveforms are shown in Fig. 4. A relation among the smart element's voltages and before (V_M) and after (V_m) the inversion process, the rectified voltage V_{DC} and the electrical quality factor Q_i is given in Eq. (11). Another relation between V_M and V_m for the open circuit evolution of smart element's voltages, is given in Eq. (12). By considering that during a semi-period of vibration T/2, input energy of the rectifier and the consumed energy by the equivalent load resistance R_L are equal, that it results to Eq. (13) [5, 12, 17].

$$V_m - V_{DC} = -(V_M - V_{DC})e^{\frac{-\pi}{2Q_i}}, \tag{11}$$

$$V_M = -V_m + \frac{2\alpha_2 u_m}{c_0} + \frac{2\alpha_1 \theta_m}{c_0}, \tag{12}$$

$$V_{DC} \int_{t_0}^{t_0+\frac{T}{2}} Idt = c_0 V_{DC}\left(V_M + V_m\right) = \frac{\pi}{R_L \omega} V^2{}_{DC}. \tag{13}$$

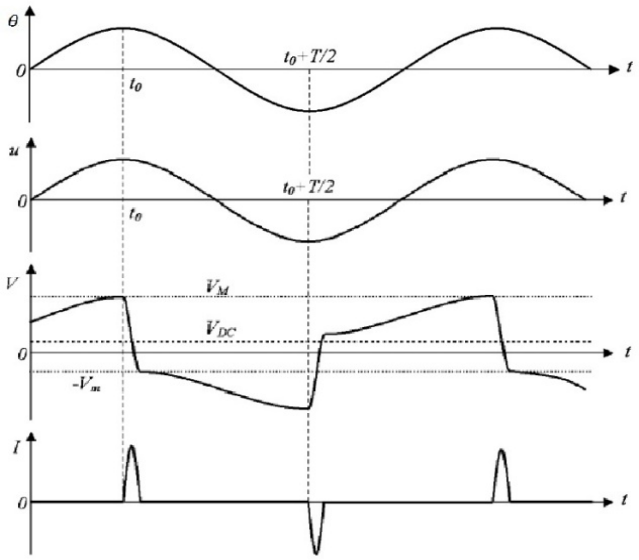

Fig. 4. Series-SSHI interface: temperature, displacement, voltage and electrical current waveforms [5, 11, 17].

An expression of the load voltage V_{DC} as a function of the temperature amplitude θ_m, the displacement amplitude u_m, and the equivalent load resistor R_L and the other system parameters is described in Eq. (14), by combining Eqs. (11)–(13). Similar to parallel SSHI Equations, the average harvested power, maximum harvested power and optimal equivalent load resistance R_{opt}, could be expressed in Eqs. (15)-(17):

$$V_{DC} = \frac{2R_L\omega(1+e^{\frac{-\pi}{2Q_i}})}{\pi(1-e^{\frac{-\pi}{2Q_i}}) + 2R_L C_0 \omega(1+e^{\frac{-\pi}{2Q_i}})}\left(\alpha_2 U_m + \alpha_1 \theta_m\right), \tag{14}$$

$$P = \frac{V_{DC}^2}{R_L} = \frac{4R_L\omega^2(1+e^{\frac{-\pi}{2Q_i}})^2}{\left(\pi(1-e^{\frac{-\pi}{2Q_i}}) + 2R_L C_0\omega(1+e^{\frac{-\pi}{2Q_i}})\right)^2}(\alpha_2 U_m + \alpha_1\theta_m)^2, \tag{15}$$

$$P_{\max} = \frac{\omega}{2\pi C_0}\frac{(1+e^{\frac{-\pi}{2Q_i}})}{(1-e^{\frac{-\pi}{2Q_i}})}\left(\alpha_2 U_m + \alpha_1\theta_m\right)^2, \tag{16}$$

$$R_{opt} = \frac{\pi}{2C_0\omega}\frac{(1-e^{\frac{-\pi}{2Q_i}})}{(1+e^{\frac{-\pi}{2Q_i}})}. \tag{17}$$

3. Numerical results

Numerical results for PZT and PMN-0,25PT elements with both energy harvesting methods is shown in following part. As shown in Fig. 5, assumed that a cantilever beam equipped with smart elements, is under vibration and heat stimulations. Mechanical and heat forces are exerted sinusoid with the same frequency. Properties of smart elements and external stimulations are shown in Table 1.

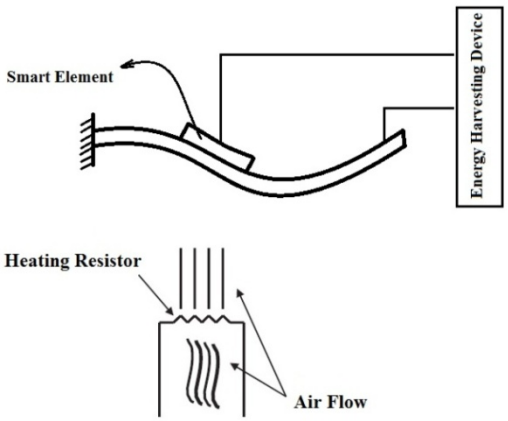

Fig. 5. Schematic diagram of the Hybrid micro generator.

Table 1. Specifications of external stimulations and smart elements.

	PZT - ceramic	PMN-0.25PT ceramic
Thickness	0.3 *mm*	1 *mm*
Area of elements	5400 mm^2	1260 mm^2
Frequency	20 *Hz*	20 *Hz*
Q_i	3	3
C_0	177 *nF*	23.417 *nF*
α_1	2.8782×10^{-6} *N/V*	9.4×10^{-67} *N/V*
α_2	0.00414 *C/°K*	0.001 *C/ °K*
u_m	2 *mm*	2 *mm*
θ_m	0.5 *°C*	0.5 *°C*

As already mentioned, results for PZT and PMNT-0.25PT are shown in Figs. 6 and 7 by applying sinusoidal vibration and heat with the same frequency, respectively. Results are presented for hybrid energy harvesting and piezo-energy harvesting, to show the positive effect of hybrid energy harvesting.

According to data in Fig. 6 maximum harvested powers by PZT elements at 20 *Hz* and Q_i =3 are 6.049 *mW* and 4.816 *mW* for parallel and series circuits, respectively, whereas these are 8.335 *mW* and 6.636 *mW* for hybrid harvesting energy. In accord with Fig. 7 these maximum harvested powers for PMN-0.25PT elements are 2.667 *mW* and 2.816 *mW* for parallel and series SSHI just by using piezoelectric effect, while these amounts of harvested power increase to 4.069 *mW* and 3.239 *mW* by using hybrid technique.

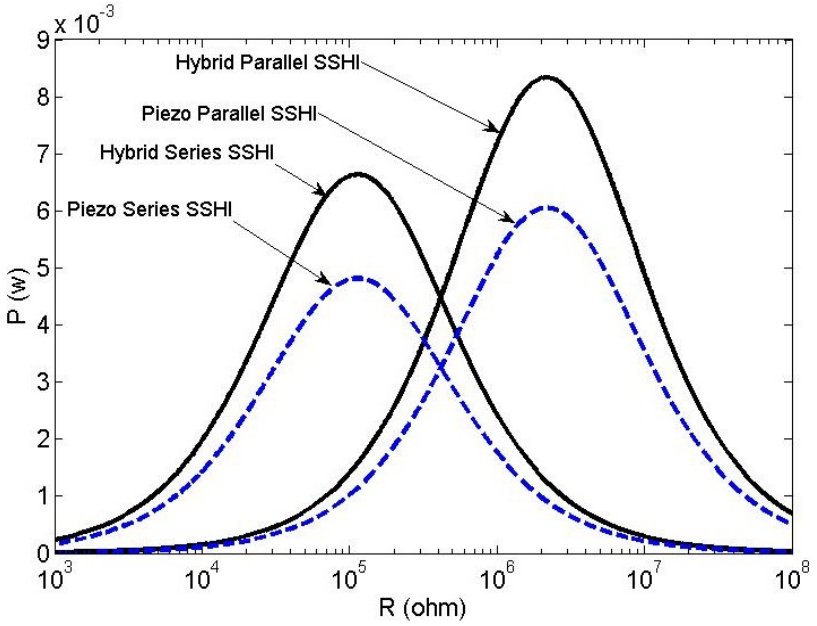

Fig. 6. Harvested electrical power as a load resistance, for PZT elements (Solid line: Hybrid energy harvesting & dash: Piezo-energy harvesting).

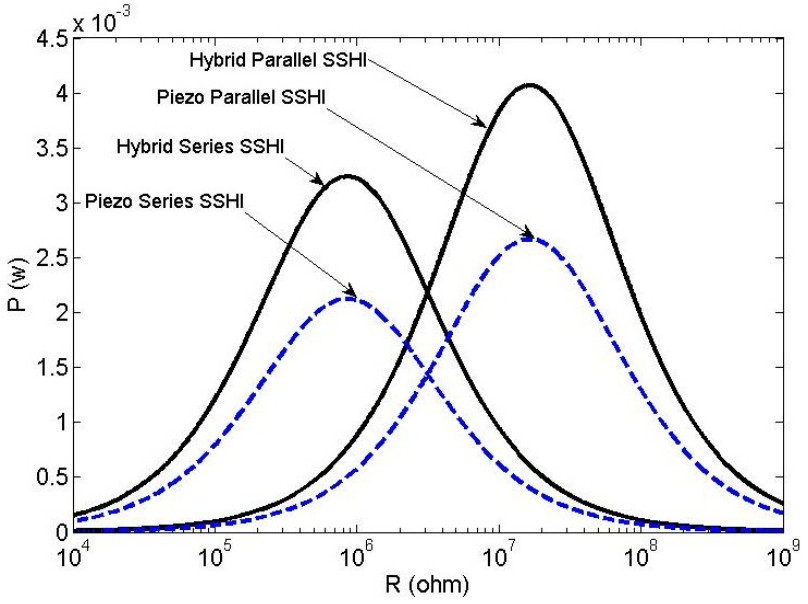

Fig. 7. Harvested electrical power as a load resistance, for PMN-0.25PT elements (Solid line: Hybrid energy harvesting & dash: Piezo-energy harvesting).

Thus, by using a hybrid energy harvesting technique, maximum harvested power increases almost 38 % and 53 % for PZT and PMN-PT elements, respectively. It should be noted that as the Figs. 6 and 7 shows, using hybrid energy harvesting doesn't change optimal load resistance, compared with its value in piezo-energy harvesting. This set of changes is shown in Table 2.

In the second part, the effect of three important parameters-temperature amplitude, vibration amplitude, and frequency-are studied.

Table 2. Result of harvesting energy by PZT and PMN-0.25PT.

Element	Interface circuit	Optimal resistance load	Maximum harvested power by piezo-effect	Maximum harvested power by hybrid-effect	Increase in harvested power
PZT	Parallel SSHI	2.1771 $M\Omega$	6.049 mW	8.335 mW	37.79 %
	Series SSHI	0.1136 $M\Omega$	4.816 mW	6.636 mW	33.79 %
PMN-0.25PT	Parallel SSHI	16.456 $M\Omega$	2.667 mW	4.069 mW	52.56 %
	Series SSHI	0.8585 $M\Omega$	2.816 mW	3.239 mW	52.49 %

Figures 8-10 show harvested power as the temperature amplitude, vibration amplitude and frequency, for each Parallel and series SSHI, respectively.

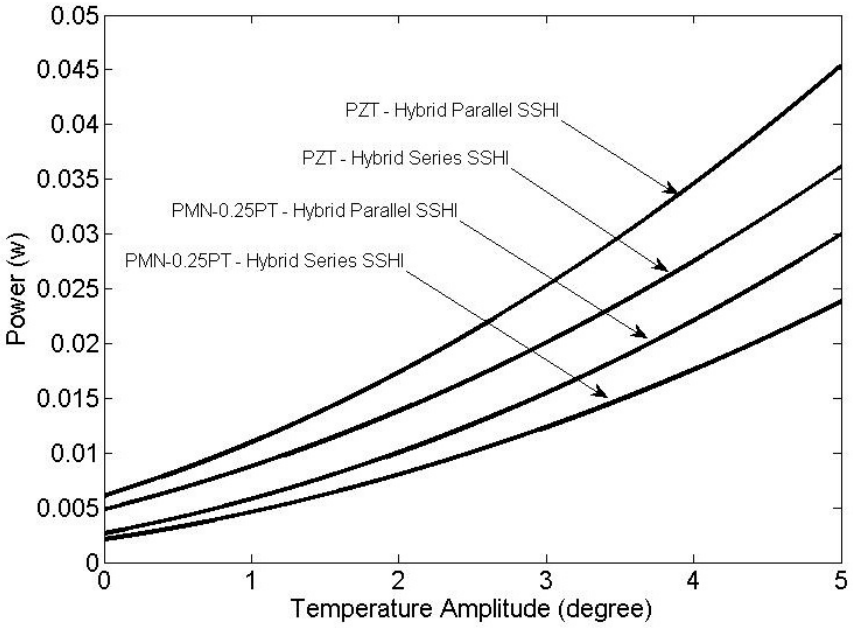

Fig. 8. Harvested electrical power as a temperature amplitude, for PMN-0.25PT elements.

Regard to results in Figs. 6 and 7, harvested power of PZT elements is higher than PMN-0.25PT elements due to the higher piezoelectric coefficient. It is proven that piezoelectric effect has a more portion in harvesting energy, compared to pyroelectric effect. As the Figure 8 shows harvested power is increased by growing temperature amplitude. These

changes are almost similar for all interface circuits, and for PZT and PMN-0.25PT elements. The same trend is observed for changes of vibration amplitude, which are presented in Fig. 9. The difference between the slopes of these curves is explainable by considering equations of harvesting circuits and piezoelectric and pyroelectric coefficients for each element. In addition, Figure 10 shows an increase of stimulation's frequency led to harvesting more electrical power. With respect to preceding reasons, PZT elements harvest more electrical power. Although, increasing frequency between 0 *Hz* to 50 *Hz* has a significant positive effect on harvesting energy; at frequencies above 200 *Hz* diagrams remain almost steady as the frequency changes.

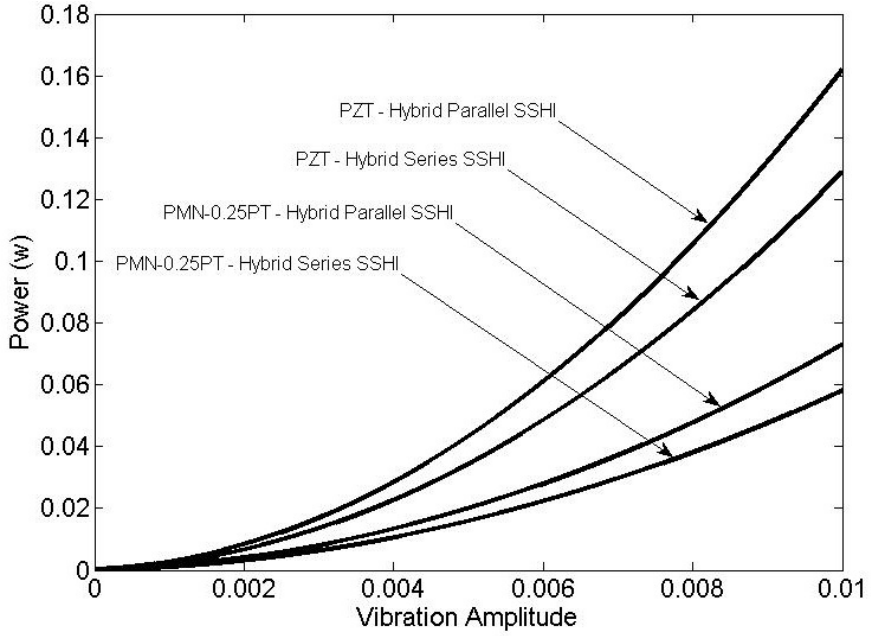

Fig. 9. Harvested electrical power as a vibration amplitude, for PMN-0.25PT elements.

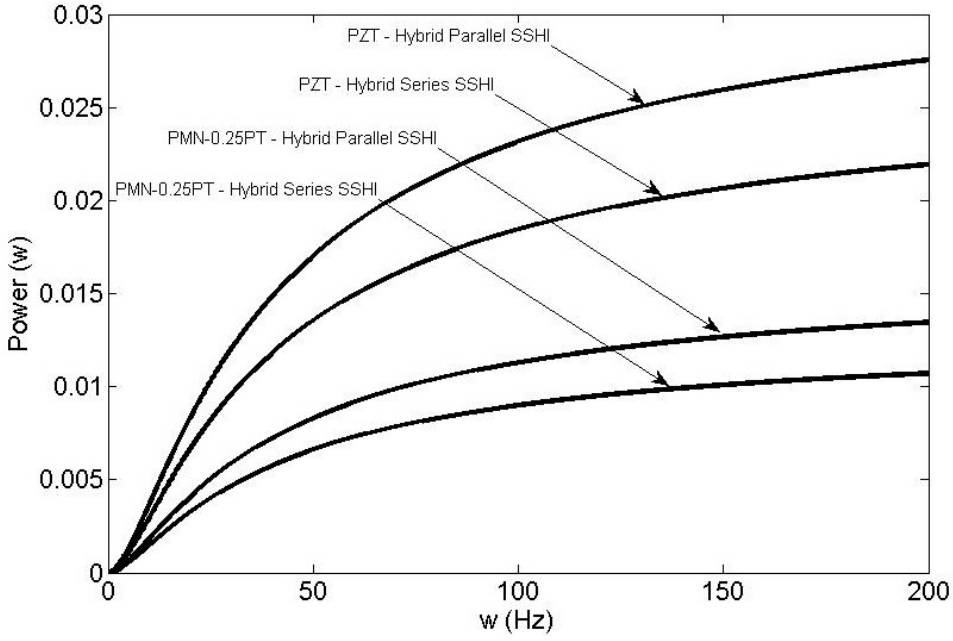

Fig. 10. Harvested electrical power as a frequency, for PMN-0.25PT elements.

To check different effects of these changes, maximum harvested power for each method is calculated by assuming doubling these parameters. The set of these changes is presented in Table 3.

In harvesting energy circuits low electrical current and optimal resistance load is desirable in energy harvesters, therefore, series SSHI is preferred. Refer to recent developments in microelectronic technology, by improving electrical quality factor of devices, this amount of harvested energy will increase.

Table 3. Effect of doubling effective parameters on harvested power.

Smart element	Increase in harvested power by doubling temperature amplitude	Increase in harvested power by doubling vibration amplitude	Increase in harvested power by doubling stimulation frequency
PZT	32 %	243 %	78 %
PMN-0.25PT	42 %	227 %	78 %

4. Conclusions

Mechanical vibrations accompany with temperature gradients exist in many industrial locations. In this paper it has been proven that hybrid energy harvesting energy by pyroelectric and piezoelectric effect, simultaneously, increases almost 38 % and 53 % more power as it does harvest by just piezoelectric effect. Using a hybrid technique does not change the optimal resistance load Numerical results show that this method is more effective for smart elements, which pyroelectric coefficient of them are higher than their piezoelectric coefficient. Consequently, PMN-0.25PT has better performance compared with two smart elements has studied in this paper. Vibration, temperature amplitude, and stimulation frequency have direct relation to hybrid harvested power. Among these effective parameters, increasing vibration amplitude has more positive effect resulted from more portion of piezoelectric effect in harvesting energy, compared with results from pyroelectric effect.

References

[1] A. Khodayari, S. Pruvost, G. Sebald, D. Guyomar, S. Mohammadi // *IEEE Trans. Ultrason. Ferroelectr. Freq. Control* **56** (2009) 693.
[2] V. Raghunathan, C. Schurgers, S. Park, M.B. Srivastava // *IEEE Signal Process. Mag.* **9** (2002) 40.
[3] S. Roundy, E.S. Leland, J. Baker, J. Carleton, E. Reilly, E. Lai, B. Otis, J.M. Rabeay, P.K. Wright, V. Sandararajan // *IEEE Pervasive Comput.* **4** (2005) 28.
[4] E. Lefeuvre, A. Badel, C. Richard, D. Guyomar // *Proc. SPIE 5390, Smart Structures and Materials 2004: Smart Structures and Integrated Systems*, **379** (July 26, 2004); doi:10.1117/12.532709; http://dx.doi.org/10.1117/12.532709.
[5] E. Lefeuvre , A. Badel, C. Richard, L. Petit, D. Guyomar // *Sensors and Actuators A* **126** (2006) 405.
[6] W. Clarck, Changki Mo // *Smart Mater. Struct.* **19** (2010) 025016.
[7] S. Roundy, P.K. Wright // *Proceedings of Smart Mater. Struct.* **13** (2004) 1131.
[8] D. Guyomar, S. Pruvost, G. Sebald // *IEEE Trans. Ultrason. Ferroelectr. Freq. Control* **55** (2008) 279.
[9] G. Sebald, S. Pruvost, D. Guyomar // *Smart Mater. Struct.* **17** (2008) 015012.
[10] G. Ottman, H. Hofmann, A. Bhatt, G. Lesieutre // *IEEE Trans. Power Electron.* **17 (5)** (2002) 669.

[11] G. Ottman, H. Hofmann, A. Bhatt, G. Lesieutre // *IEEE Trans. Power Electron.* **18** (2003) 696.
[12] D. Guyomar, G. Sebald, E. Lefeuvre, A. Khodayari // *J. Intell. Mater. Syst. Struct.* **20** (2009) 256.
[13] S. Roundy, P.K. Wight, J. Rabaey // *Comput. Commun.* **26** (2003) 1131.
[14] S. Horwitz, A. Kasyap, F. Liu, D. Johnson, T. Nishida, K. Ngo, M. Sheplak, L. Cattafesta, In: *1st AIAA Flow Control Conference (*St. Louis, MO, June 24–26, 2002), paper 2002-2702.
[15] M.H. Lee, R. Guo, A.S. Bhalla // *J. Electroceram.* **2** (1998) 229.
[16] R. Radebaugh, W.N. Lawless, J.D. Siegwarth, A.J. Morrow // *Cryogenics* **19** (1979) 187.
[17] D. Guyomar, A. Badel, E. Lefeuvre, C. Richard // *IEEE Trans. Ultrason. Ferroelectr. Freq. Control* 52 (2005) 584.
[18] A. Badel, A. Benayard, E. Lefeuvre L. Lebrun, C. Richard, D. Guyomar // *IEEE Trans. Ultrason. Ferroelectr. Freq. Control* **53** (2006) 673.
[19] G. Sebald, E. Lefeuvre, D. Guyomar // *IEEE Trans. Ultrason. Ferroelectr. Freq. Control* **55** (2008) 538.
[20] L. Garbuio, M. Lallart, D. Guyomar, C. Richard, D. Audigier // *IEEE Trans. On. Indust. Elect.* **56** (2009) 523.
[21] D. Guyomar, Y. Jayet, L. Petit, E. Lefeuvre, T. Monnier, C. Richard, M. Lallart // *Sens. Actuators A* **138** (2007) 151.
[22] E. Lefeuvre, D. Audigier, C. Richard, D. Guyomar // *IEEE Trans. Power Electron.* **22** (2007) 2018.
[23] E. Lefeuvre, A. Badel, C. Richard, D. Guyomar // *J. Intell. Mater. Syst. Struct.* **16** (2005) 865.